



## Hydrodynamic and mass spectrometry analysis of nearly-intact human fibrinogen, chicken fibrinogen, and of a substantially monodisperse human fibrinogen fragment X

Barbara Cardinali<sup>a</sup>, Aldo Profumo<sup>a</sup>, Anna Aprile<sup>a</sup>, Olwyn Byron<sup>b</sup>, Gordon Morris<sup>c</sup>, Stephen E. Harding<sup>c</sup>, Walter F. Stafford<sup>d</sup>, Mattia Rocco<sup>a,\*</sup>

<sup>a</sup> *Biopolimeri e Proteomica, Istituto Nazionale per la Ricerca sul Cancro (IST), Largo R. Benzi 10, I-16132 Genova, Italy*

<sup>b</sup> *Division of Infection and Immunity, Institute of Biomedical and Life Sciences, University of Glasgow, G12 8QQ, Glasgow, Scotland, UK*

<sup>c</sup> *The National Centre for Macromolecular Hydrodynamics, School of Biosciences, University of Nottingham, Sutton Bonington LE12 5RD, UK*

<sup>d</sup> *AUC Research Laboratory, Boston Biomedical Research Institute, Watertown, MA 02472, USA*

### ARTICLE INFO

#### Article history:

Received 30 September 2009  
and in revised form 15 October 2009  
Available online 22 October 2009

#### Keywords:

Blood coagulation  
Plasma proteins  
Analytical ultracentrifugation  
Light scattering  
Differential pressure viscometry  
Fibrinogen degradation products

### ABSTRACT

The shape and solution properties of fibrinogen are affected by the location of the C-terminal portion of the A $\alpha$  chains, which is presently still controversial. We have measured the hydrodynamic properties of a human fibrinogen fraction with these appendages mostly intact, of chicken fibrinogen, where they lack 11 characteristic 13-amino acids repeats, and of human fragment X, a plasmin early degradation product in which they have been removed. The human fibrinogen/fragment X samples were extensively characterized by SDS-PAGE/Western blotting and mass spectrometry, allowing their composition to be precisely determined. The solution properties of all samples were then investigated by analytical ultracentrifugation and size-exclusion HPLC coupled with multi-angle light scattering and differential pressure viscometry detectors. The measured parameters suggest that the extra repeats have little influence on the overall fibrinogen conformation, while a significant change is brought about by the removal of the C-terminal portion of the A $\alpha$  chains beyond residue A $\alpha$ 200.

© 2009 Elsevier Inc. All rights reserved.

### Introduction

Fibrinogen (FG)<sup>1</sup> is a high molecular weight (~340,000), centrosymmetric, dimeric glycoprotein found in the blood of vertebrates, where physiologically plays a critical role in the coagulation system [1,2]. Each half of the molecule consists of three polypeptide chains, called A $\alpha$ , B $\beta$  and  $\gamma$ , whose six N-termini are contained in a central, symmetric globular region (“E-region”) [2–4]. Two triple coiled-coil connectors join this region to two outer globular regions (“D-regions”), formed by the C-terminal parts of the B $\beta$  and  $\gamma$  chains, each folding into independent domains [2–4]. The triple coiled-coil con-

nectors are held in register at their beginning and end by two disulfide bridge rings [3–7]. At the end of each coiled-coil, after the second disulfide ring, the A $\alpha$  chain reverses direction, forming a fourth coiled helix continuing for about half of the connector’s length [6,7]. Thereafter, the location of the C-terminal parts of the A $\alpha$  chains ( $\alpha$ C regions) is instead still controversial, ranging from partially free-swimming appendages [3,7], to forming a fourth globular region positioned on top of the central one [8–13]. Interestingly, there is a wide variation in the length of this portion of the A $\alpha$  chain among vertebrate species [14–20], mostly depending on the number of several 13-amino acids imperfect tandem repeats. In particular, ten such repeats were originally identified in the human species’ A $\alpha$  chain [14], which has 610 residues in the mature form, but at least another repeat was later reported [21]. Instead, the repeats are completely absent in the chicken A $\alpha$  chain, which has only 476 residues [18]. In Fig. 1, an alignment of the human and chicken sequences for the A $\alpha$  chain residues after the second disulfide ring is presented, where the definition of a possible additional, non-canonical repeat is also suggested. In contrast, the B $\beta$  and  $\gamma$  chains have pretty much the same length in humans and chickens, containing 461/463 and 411/409 residues, respectively [7,24,25]. The  $\alpha$ C regions are very susceptible to proteolytic attack, and their complete removal by

\* Corresponding author. Fax: +39 0105737 325.

E-mail addresses: [barbara.cardinali@istge.it](mailto:barbara.cardinali@istge.it) (B. Cardinali), [aldo.profumo@istge.it](mailto:aldo.profumo@istge.it) (A. Profumo), [anna.aprile@istge.it](mailto:anna.aprile@istge.it) (A. Aprile), [o.byron@bio.gla.ac.uk](mailto:o.byron@bio.gla.ac.uk) (O. Byron), [Gordon.Morris@nottingham.ac.uk](mailto:Gordon.Morris@nottingham.ac.uk) (G. Morris), [Steve.Harding@nottingham.ac.uk](mailto:Steve.Harding@nottingham.ac.uk) (S.E. Harding), [stafford@bbri.org](mailto:stafford@bbri.org) (W.F. Stafford), [mattia.rocco@istge.it](mailto:mattia.rocco@istge.it) (M. Rocco).

<sup>1</sup> *Abbreviations used:* FG, fibrinogen; hFG, human fibrinogen; hFrX, human fibrinogen fragment X; hHMW-FG, human high molecular weight fibrinogen; hLMW-FG and hLMW'-FG, human low molecular weight (prime) fibrinogen; AUC, analytical ultracentrifugation; SEC, size-exclusion chromatography; SE-HPLC, size-exclusion high-performance liquid chromatography; MALLS, multi-angle laser light scattering; DPV, differential pressure viscometry; TIC, total ion chromatogram.

H166	S R A L A R E V D L K D Y E D Q Q K Q L E Q V I A	H190	4 <sup>th</sup> helix on coiled coil
C167	A R S F D Y Q V D K E G Y D N I Q K H L T Q A S S	C191	
H191	K D L L P S R D R Q H L P L I K M K P V P D L - V P G	H216	
C192	I D M H P D F Q T T T L S T L K M R P L K D S N V P E	C218	4 <sup>th</sup> helix on coiled coil
H217	N F K S Q L Q K V P P E W K A L T D M P Q	H237	Predicted mostly helix
C219	H F K L K P S P E M Q A M S A F N N I K Q	C239	
H238	M R M E L E R P G G N E I T	H251	Predicted mostly sheet
C240	M Q V V L E R P E T D H V A	C253	
H252	R G G S T S Y G - T G S E	H263	Repeat I
H264	T E S P R N P S S A G S W	H276	Repeat II
H277	N S G S S G P G S T G N R	H289	Repeat III
H290	N P G S S G T G G T A T W	H302	Repeat IV
H303	K P G S S G P G S A G S W	H315	Repeat V
H316	N S G S S G T G S T G N Q	H328	Repeat VI
H329	N P G S P R P G S T G T W	H341	Repeat VII
H342	N P G S S E R G S A G H W	H354	Repeat VIII
H355	T S E S S V S G S T G Q W	H367	Repeat IX
H368	H S E S - G S F R P D S P	H379	Repeat X
H380	G S G N A R P N N P D - W	H391	Repeat XI
H392	G T F E E V S G N V - S P	H403	Repeat XII?
C254	- - - E A R G D - S S P	C261	
H404	G T R R E Y H T E K L V T S K G D K E L R	H424	Predicted mostly sheet
C262	S - - - - H T G K L I T S S H R R E S P	C277	
H425	T G K E K V T S G S T T T T R R S C S K T V T K T V I - G	H452	Start globular region
C278	S L V D K T S S A S S V - - - H R C T R T V T K K V I S G	C303	(bovine NMR)
H453	P D G H K E V T K E V V T S E D G S D C P E A M D - - - -	H477	
C304	P D G P R E E I V E K M V S S D G S D C S H L Q G G R E E G	C332	
H478	- L G T L S G I G T L D G F R H R H P D E A A F F D ↓ T A S	H505	(↓ = end bovine NMR)
C333	S T Y H F S G T G D F H K L D R L L P D L E S F F T H D S	C361	
H506	T G K T F P G F F S P - - - - M L G E F V S E T E S R G	H529	
C362	V S T S S R H S I G S S T S S H V T G A G S S H L G T G G	C390	
H530	S E S G I F T N T K E S S S H H P G I A E F P S - - R G K	H556	
C391	K D K - - F T D L G E E E E D D F G G L Q - P S G F A A G	C416	
H557	S S S Y S K Q F - - T S S T S Y N R G D S T F E S K S Y K	H583	End globular region
C417	S A S H S K T V L T S S S S S F N K G G S T F E T K S L K	C445	
H584	- - - M A D E A G S E A D H E G T H S T K R G H A K S - R P V	H610	C-terminal
C446	T R E T S E Q L G G V Q H D Q S A E D T P D F K A R S F R P A	C476	

**Fig. 1.** Alignment of the human (H) and chicken (C)  $\alpha$  chain C-terminal region after the second disulfide ring, as produced by T-COFFEE version 5.05 (<http://www.tcoffee.org>) [22]. Some features are indicated on the right side; the secondary structure predictions were made with Jpred3 (<http://www.compbio.dundee.ac.uk/www-jpred/>) [23]. Mature proteins numbering.

plasmin generates a FG species known as “fragment X” (FrX) [26], which also lacks the first ~54 residues of the  $\beta$  chain [27] (the N-terminus contains a thrombin-cleavable sequence called fibrinopeptide B, hence the name change from  $B\beta$  to  $\beta$ ; a similar sequence, fibrinopeptide A, is at the N-terminus of the  $\alpha$  chain). A similar species, but with an uncleaved  $B\beta$  N-terminus, is found in normal plasma together with nearly-intact FG; they are often referred to as “fraction I-8” and “fraction I-4”, respectively [28].

Over the past ~10 years, great advancements have been made in determining the structure of fibrinogen, mainly by X-ray crystallography, e.g. [6,7,29–35]. In particular, the structure of intact chicken fibrinogen at 2.7 Å resolution was determined, but the  $\alpha$  chain could not be traced beyond residue Glu218 [7]. However, two nearly symmetrical electron density blobs were defined be-

tween the elongated, staggered FG molecules in the crystals, sideways to the  $\beta$ C-domains, above the second half of the coiled-coil of a molecule, and below the central region of the preceding molecule (see Fig. 2 in [7]). Likewise, the  $\alpha$ C regions could not be resolved in the recent crystal structure of intact human FG [35]. Structural studies have also been performed on the last ~200 residues of the  $\alpha$  chain ( $\alpha$ C-domain), identified as a likely globular region by calorimetry [36,37]. In particular, a recent NMR study has presented the structure of a bovine  $\alpha$ C-domain recombinant fragment corresponding to the human 425–505 and chicken 278–361 residues [38].

The location of such a large portion of the  $\alpha$  chain could clearly affect the shape and the solution behavior of FG. In order to determine their contribution, we have measured the hydrodynamic

properties of three different FG species differing by the length of the  $\alpha$ C region, a high molecular weight human FG fraction (hHMW-FG), an almost monodisperse human fragment X (hFrX), and a crystallography-grade intact chicken FG sample (cFG, generously provided by Prof. R.F. Doolittle, UCSD, La Jolla, CA, USA). The hHMW-FG and hFrX samples were extensively characterized by SDS–PAGE/Western blot analyses and by mass spectrometry, allowing their composition to be determined with great confidence. The weight-averages sedimentation coefficient ( $s_{20,w}^0$ ) and intrinsic viscosity ( $[\eta]_w$ ) were then determined for all the samples, respectively by analytical ultracentrifugation (AUC) and by on-line differential viscometry following size-exclusion high-pressure liquid chromatography (SE-HPLC). A multi-angle laser light scattering (MALLS) detector, also present in the SE-HPLC set-up, provided estimates of the rms z-average radius of gyration ( $\langle R_g^2 \rangle_z^{1/2}$ ) and of the mean-weight molecular weight ( $\langle M \rangle_w$ ) of the samples.

## Materials and methods

### General

All chemicals were reagent grade from Merck (distributed by VWR International, Milano, Italy; <http://www.merck-chemicals.com/>), unless otherwise stated, and double-distilled water was used in the preparation of all the solutions. Lyophilized human fibrinogen (hFG; plasminogen depleted, type FIB1 from Enzyme Research Laboratories, South Bend, IN; <http://www.enzymere-search.com/>; or Cat# 341578 from Calbiochem, Merck; <http://www.merckbiosciences.co.uk/home.asp>) was reconstituted at 37 °C at a nominal concentration of 20 mg/ml in the original buffer (sodium citrate–HCl 20 mM, pH 7.4) plus 10 kallikrein inhibitor units (KIU)/ml of aprotinin (serine protease inhibitor, Sigma–Aldrich, St. Louis, MO; <http://www.sigmaaldrich.com/sigma-aldrich/home.html>). It was then dialyzed twice against Tris Buffered Saline (TBS; tris(hydroxymethyl)aminomethane 50 mM, NaCl 104 mM, aprotinin 10 KIU/ml, pH 7.4), divided in aliquots, snap-frozen in liquid N<sub>2</sub>, and stored at –80 °C. The unfractionated hFG concentration was determined from the absorbance at 280 nm, after correction for scattered light at 320 nm, using a specific adsorption coefficient  $E^{280}$  of 1.51 ml mg<sup>–1</sup> cm<sup>–1</sup> [39]. A DU640 spectrophotometer (Beckman Coulter, Fullerton, CA; <http://www.beckman-coulter.com>) was used for all spectrophotometric operations. cFG was received as frozen aliquots in NaCl 150 mM, imidazole 50 mM, pH 7.0 (shipped in dry ice), and was immediately stored at –80 °C. Upon thawing at 37 °C, its concentration was determined using  $E^{280} = 1.34$  ml mg<sup>–1</sup> cm<sup>–1</sup>, calculated from its amino acid composition (UniProt sequences P14448-2, Q02020, and Q93568; <http://www.uniprot.org>) and carbohydrate content (four biantennary Man<sub>3</sub>GlcNAc<sub>4</sub>Gal<sub>2</sub>NeuNAc<sub>2</sub> putative chains like in the human species) using PROMOLP [40].

### Electrophoresis and Western blotting

Quality control and characterization of the samples was done by various polyacrylamide (PAA) gel electrophoresis in the presence of sodium dodecyl sulphate (SDS) methods (SDS–PAGE) [41], employing 10 × 8 cm, 1.0 mm or, for blotting, 0.75 mm thick gels run in a SE 250 Mighty Small II apparatus (Hofer Inc., Holliston, MA; <http://www.hoferinc.com/>). Acrylamide, *N,N'*-methylenebis-acrylamide and ammonium persulfate were from Bio-Rad (Hercules, CA; <http://www.bio-rad.com/>), while *N,N,N',N'*-tetramethylethylenediamine (TEMED) was from Sigma–Aldrich. Electrophoresis samples were prepared so to have ideally 50 µg protein in 100 µl of Tris 125 mM (not counting that originally present in the sample), SDS 2.5%, pH 6.8, with or without 5% dithiothreitol

(DTT, Sigma–Aldrich) as a reducing agent. After boiling for 5 min, 100 µl of 0.2% bromophenol blue (Bio-Rad) in 20% glycerol were added, and 10–20 µl samples were loaded in each gel well. Two type of PAA gels were used, without or with 8.5 M urea. Without urea, the gels consisted of a PAA 3% T (total monomer concentration), 2.6% C (crosslinker w/w%) in Tris 135 mM, SDS 0.1%, pH 6.8 stacking zone (~1 cm), and of a resolving zone with various T percentages (8–12.5%, all with 2.6% C) in Tris 380 mM, SDS 0.1%, pH 8.8. The running buffer was Tris 25 mM, glycine 192 mM, SDS 0.1%, pH 8.3, and the electrophoresis was carried out with constant current (30 mA/gel) until the tracking dye eluted from the bottom of the gel. The urea-containing gels consisted of a stacking zone with PAA 3.5% T–5% C in urea 2.2 M, Tris 110 mM, H<sub>3</sub>PO<sub>4</sub> 90 mM, SDS 0.11%, pH 5.7, followed by a resolving zone with PAA 3.2% T–5% C with urea 8.5 M in the same buffer. The running buffer was NaH<sub>2</sub>PO<sub>4</sub>/Na<sub>2</sub>HPO<sub>4</sub> 0.1 M, SDS 0.1%, pH 7.1, and the gels were pre-run at 100 V (constant voltage mode) for 10 min before sample loading, which was done after diluting 1:1 the samples prepared as described above with urea 8 M, SDS 1% in water. The electrophoresis was then carried out at constant voltage, 50 V for 45 min, and then 100 V until the tracking dye eluted from the bottom. Unstained molecular weight markers were from Bio-Rad (low range, cat. 161–0304; broad range, cat. 161–0317).

The gels were stained with 0.1% Coomassie Blue R-250 (Bio-Rad) in 45% CH<sub>3</sub>OH, 10% CH<sub>3</sub>COOH, and destained with 20% CH<sub>3</sub>OH, 7.5% CH<sub>3</sub>COOH, or electrophoretically blotted on 0.45 µm pore-size nitrocellulose membranes (Hybond-C, Amersham, GE Healthcare, Chalfont St. Giles, UK; <http://www.gehealthcare.com/worldwide.html>) for immunostaining with specific antibodies (Western blotting), using a Mini Protean II cell (Bio-Rad). The transfer buffer consisted of Tris 25 mM, glycine 190 mM, CH<sub>3</sub>OH 20%, pH 8.3. The IgM Y18 monoclonal antibody (MAB) (a generous gift of Dr. T. Kooistra, Gaubius Laboratory TNO-PG, Leiden, The Netherlands), directed against an epitope on the fibrinopeptide A [42], was employed to recognize the A $\alpha$  chains, while for the  $\gamma$  chains the IgG1 mouse MAb J88B, directed against the  $\gamma$ 63–70 sequence [43] (a generous gift of P.J. Simpson-Haidaris, University of Rochester, Rochester, NY) was used. Color development was done with horseradish peroxidase-conjugated goat anti-mouse IgM and IgG1 secondary antibodies (SouthernBiotech, Birmingham, AL; <http://www.southernbiotech.com/>), respectively, and 4-chloro-1-naphthol (Fluka Chemie, Sigma–Aldrich) as a substrate. Dual color, Precision Plus recombinant molecular weight standards (cat. 161–0374, Bio-Rad) were used as markers.

Digital images of the gels and blots were acquired at 43 µm resolution with a GS-800 Calibrated Densitometer (Bio-Rad), using appropriate filters, with the Quantity One (version 4.6.1) software (Bio-Rad), and saved in TIFF format. Optical density (OD) profiles for each lane were determined on these images with the OneDscan software (Scanalytics, CSP, Billerica, MA) followed by deconvolution of overlapping peaks with PeakFit v.4 (Jandel Scientific, now distributed by Systat Software Inc., Richmond, CA; <http://www.sigmaplot.com/>), as previously reported [44].

### hHMW-FG and hLMW-FG preparation

The procedure described here is an adaptation of a protocol kindly provided by Dr. M. De Maat (Erasmus MC, Rotterdam, NL), based on previously reported methods [45,46]. hFG in TBS buffer was thawed at 37 °C, diluted to 7–8 mg/ml, and 5–10 ml dialyzed twice at 4 °C against 500 ml of imidazole 0.15 M, aprotinin 10 KIU/ml, pH 7.35 buffer. After dialysis, the hFG concentration was adjusted to 5 mg/ml and the solution equilibrated at room *T* (~22 °C). Saturated (NH<sub>4</sub>)<sub>2</sub>SO<sub>4</sub> was then added, drop by drop under gentle stirring, to a final concentration of 19%. The mixture was then incubated for 10 min under gentle stirring and then centri-

fused for 10 min at 3000 g in a 6G Beckman centrifuge. The pellet was resuspended in 1/3 of the initial volume using NaCl 0.15 M, and the precipitation step was repeated once again. After centrifugation, the pellet containing the hHMW-FG fraction was dissolved in 1/10 of the initial volume of NaCl 0.15 M. The concentration of  $(\text{NH}_4)_2\text{SO}_4$  in the supernatant derived from the first precipitation was increased to 22% using the procedure described above. After centrifugation, the pellet was discarded, the supernatant was collected and the  $(\text{NH}_4)_2\text{SO}_4$  concentration was increased to 24%. The pellet obtained from this step contains the intermediate hLMW-FG fraction and was dissolved in NaCl 0.15 M in 1/20 of the original volume of this step. The concentration of  $(\text{NH}_4)_2\text{SO}_4$  in the supernatant from the last precipitation step was then increased to 26%. After centrifugation, the pellet was discarded and the  $(\text{NH}_4)_2\text{SO}_4$  concentration in the supernatant was brought to 30%. Finally, after the last centrifugation the supernatant was discarded and the pellet, containing the hLMW'-FG fraction, was dissolved in NaCl 0.15 M, in 1/40 of the original volume of this step.

The hLMW-FG and hLMW'-FG fractions were then dialyzed twice at 4 °C against TBS buffer without aprotinin. The hHMW-FG fraction was instead dialyzed in TBS plus 10 KIU/ml aprotinin and 10 mM AESBF (4-(2-aminoethyl) benzenesulfonyl fluoride hydrochloride; serine protease inhibitor, Sigma–Aldrich). All fractions were snap-frozen in liquid  $\text{N}_2$  and stored at –80 °C.

#### Fragment X preparation and purification

Lyophilized human plasmin (lot 41H9335, Sigma–Aldrich) was reconstituted with 1 ml of HPLC-grade water to a final nominal concentration of 10 U/ml, snap-frozen and stored in 50  $\mu\text{l}$  aliquots at –20 °C until use. The hLMW' fraction was used as the starting material for hFrX preparation, and was first dialyzed twice at 4 °C against Tris 150 mM, pH 7.8; its concentration was then adjusted to 5 mg/ml. Digestions were carried out at 22 °C by adding  $\text{CaCl}_2$  to 10 mM and 0.1 U/ml plasmin. The reaction was stopped by the addition of aprotinin to 500 KIU/ml. To determine the best reaction time, a 2 h time course experiment was performed on a small aliquot of 400  $\mu\text{l}$ . At different times, 10  $\mu\text{l}$  of the mixture were withdrawn, mixed in a new tube with the non-reducing electrophoresis sample buffer, boiled for 5 min, and then analyzed on 3.2% T PAA–urea gel. Depending on the heterogeneity of the starting hLMW'-FG fraction, the best reaction time was found to be between 10 and 20 min. Each preparative run employed 10–20 ml of hLMW'-FG, with enzyme and inhibitor properly scaled up. Plasmin was then removed from the reaction mixture by affinity chromatography using 3 ml of lysine–Sepharose 4B (Pharmacia Biotech, GE Healthcare) packed in a  $0.5 \times 10$  cm open-end column (Econo-column, Bio-Rad) and pre-equilibrated in Tris 50 mM pH 7.5, aprotinin 30 KIU/ml. Elution was done at a 5 ml/h flow rate using a peristaltic pump. The flow through plus three times the column volume was collected and concentrated to ~20–25 mg/ml using a Centriprep 50 centrifugal concentrator (Amicon, Millipore, Billerica, MA; <http://www.millipore.com/>). To determine the concentration, an extinction coefficient of  $1.69 \text{ ml mg}^{-1} \text{ cm}^{-1}$  was used, computed from the putative amino acid sequences and carbohydrate content of the hFrX chains (see Results and discussion). The lysine–Sepharose 4B resin was regenerated using 0.2 M  $\epsilon$ -amino caproic acid in Tris 50 mM, NaCl 1 M, pH 7.5. Monomeric hFrX was separated from the remaining hFG species and from more degraded proteolytic products by size-exclusion chromatography (SEC) on a  $93 \times 1.6$  cm column packed with Superdex 200 Prep Grade resin (Pharmacia Biotech), operated at 4 °C by a FPLC system (GradiFrac, HiLoad Pump P-50, UV-1 monitor, and Rec 102 recorder, Pharmacia Biotech). The loading volume was 300–450  $\mu\text{l}$ , depending on sample concentration, the flow rate was 60 ml/h, and the elution was monitored at 278 nm. Fractions of 1 ml were

collected and analyzed by SDS–urea–PAGE on 3.2% T PAA gels under non-reducing condition. Selected fractions obtained from different SEC runs were pooled and concentrated to 10 mg/ml (Centriprep 50), snap-frozen, and stored –80 °C until use.

#### Protein characterization by mass spectrometry

A hFrX reduced electrophoresis sample was subjected to preparative SDS–PAGE on a  $10 \times 8$  cm, 1.5 mm thick 12.5% T PAA gel. The identification of the Coomassie Blue-stained bands, manually excised from the gel using a sterile scalpel blade, was performed by means of peptide mass fingerprinting (PMF). In-gel digestion was avoided so that the molecular weight of the intact sample could be also determined by LC/MS. The bands were therefore placed in a Centricon holder (MWCO 3000) and the proteins were electroeluted using a Centrilon Micro-Electroeluter (Amicon Millipore) according to the manufacturer instructions. The electroeluted protein solutions were then concentrated by centrifugation (to a final volume of 60–70  $\mu\text{l}$ ) and dried in a SpeedVac centrifugal evaporator (Savant, Thermo Scientific; <http://www.thermo.com/>). A destaining step was performed to eliminate the dye [47]. Briefly, the dried samples were washed with 600  $\mu\text{l}$  of an acetone, ethanol and triethylamine (90:5:5) solution, by incubating them for 3 h on a rotating wheel at 30 rpm. After centrifugation at 16,000g for 10 min, the supernatant was discarded and the washing procedure was repeated. After the final centrifugation, the supernatants were discarded, the pellets were dried in the SpeedVac, and then dissolved in 100  $\mu\text{l}$  of a 50:50 water– $\text{CH}_3\text{CN}$  solution. The solutions were divided in two aliquots of 33 and 66  $\mu\text{l}$ , to be used for the PMF and LC/MS experiments, respectively, taken to dryness again in the SpeedVac, and stored at –20 °C until used.

Lyophilized Trypsin Gold, MS Grade (Promega, Madison, WI; <http://www.promega.com/>) was dissolved at a nominal concentration of 1  $\mu\text{g}/\mu\text{l}$  in  $\text{CH}_3\text{COOH}$  50 mM and stored in small aliquots at –80 °C. The samples intended for PMF analysis were dissolved in 20  $\mu\text{l}$  of  $\text{NH}_4\text{HCO}_3$  1%, and the approximate protein concentration in each tube was evaluated. Samples were incubated for 3 h at 37 °C with trypsin at an enzyme:protein ratio of 1:100 (w/w). At the end of incubation more trypsin was added to the tubes in order to have a final enzyme:protein ratio of 1:50, and the samples were incubated overnight at 37 °C. Tryptic digests were finally purified by loading them on ZipTips C18 (Millipore), according to the manufacturer instructions.

For atmospheric pressure/matrix-assisted laser desorption ionization-time of flight mass spectrometry analysis (AP/MALDI-TOF MS), 3  $\mu\text{l}$  of the above purified samples were mixed with 10  $\mu\text{l}$  of Agilent Matrix Solution (containing 6.2 mg/ml of  $\alpha$ -cyano-4-hydroxycinnamic acid; Agilent Technologies, Waldbronn, FRG; <http://www.home.agilent.com/>), 30  $\mu\text{l}$  of  $\text{CH}_3\text{OH}$  and 36.8  $\mu\text{l}$  of Agilent Matrix Dilution, and 1  $\mu\text{l}$  of each sample was spotted and let dry on the AP/MALDI sample plate. Mass spectra were obtained from an Agilent 6210 TOF LC/MS mass spectrometer operating in positive ion reflectron mode. All spectra were obtained randomly over the surface of the matrix spot. Agilent's MassHunter software was used to create peak lists for PMF analysis, which were searched using the Spectrum Mill MS Proteomics Workbench (Agilent Technologies) software against the complete SwissProt database. The following parameters were used in the search: taxonomy, all species; protein molecular mass, 1000–150,000. The cleavage rule for trypsin was designated and the allowance for number of missed cleavages was set at 1. The peptide tolerance did not exceed 5 ppm. Carbamidomethylation was set as fixed modification while methionine oxidation as variable modification.

To accurately define the molecular mass of each protein contained in the excised bands, we initially tried with the second aliquot of the preparative SDS–PAGE step. It was resuspended in

50  $\mu\text{l}$  of  $\text{CH}_3\text{CN}$  10%, TFA 0.1% in water, and analyzed by reverse-phase HPLC-electrospray ionization (RP-HPLC-ESI)-TOF MS utilizing a  $150 \times 1.0$  mm, 300  $\text{\AA}$  pore-size, 3.5  $\mu\text{m}$  particle size Symmetry C4 column (Waters Corp., Milford, MA; <http://www.waters.com/>). The RP-HPLC was performed on an Agilent 1200 series system, equipped with G1379B degasser, G1376A capillary pump, G1377A micro autosampler, G1316A thermostatted column holder, and G1315B diode array detector. The system was equilibrated in 10% solvent B, where solvent B was 0.1% TFA in  $\text{CH}_3\text{CN}$ , and solvent A was 0.1% TFA in water. The flow rate was 30  $\mu\text{l}/\text{min}$  and the elution was performed at 25  $^\circ\text{C}$  in this sequence: isocratic 10% B for 10 min, a linear gradient over the course of 35 min to 70% B, a linear gradient to 100% B in 15 min and finally maintained at 100% B for 15 min. After UV detection, the eluent flow was then directly sent to the ESI source of the Agilent 6210 TOF LC/MS. Internal calibration during data acquisition was performed using a TOF reference mix solution supplied by Agilent. Finally, the raw spectrum was deconvoluted to obtain the actual protein mass. Unfortunately, this approach did not produce good results, probably due to remaining SDS contamination of the samples. We then prepared and injected directly a reduced crude hFrX preparation, without any previous electrophoretic separation. An appropriate amount of urea was added to 125  $\mu\text{l}$  of the hFrX preparation (3 mg/ml in Tris 0.1 M, pH 8) to attain a final urea concentration of 8 M. The mixture was treated for 3 h at 37  $^\circ\text{C}$  with DTT at the final concentration of 15 mM. To reduce the urea concentration, a 20  $\mu\text{l}$  aliquot was then spin-dialyzed (Centricon, MWCO 3000) after dilution with 150  $\mu\text{l}$  of water. It was then directly loaded onto the C4 column for the LC/MS analysis (with the same method described above). Raw spectra were obtained from selected portion of the total ion chromatogram (TIC) and their deconvolution was performed using the following parameters: protein mass range 20,000–70,000; peak threshold 30;  $m/z$  range 750–2500. The same procedure was employed for the analysis of the  $\text{A}\alpha$ ,  $\text{B}\beta$ , and  $\gamma$  chains derived from the reduction of the hHMW-FG samples.

#### Sedimentation velocity in the analytical ultracentrifuge

Sedimentation velocity experiments were performed using a Beckman Instruments (Palo Alto, CA; now Coulter Beckman) Optima XLI Analytical Ultracentrifuge. In each experiment, sample solutions (380  $\mu\text{l}$ ) of various concentrations ( $\sim 0.1$ –1.8 mg/ml) and TBS buffer (400  $\mu\text{l}$ ) were loaded into the solution and reference channels, respectively, of seven double sector, 12 mm optical path-length cells. After loading, the samples were spun for a few minutes at 3500 rpm to check for leaks and to record an absorbance scan (250–350 nm) used to calculate the actual sample concentration in each cell. Samples were then centrifuged at 45,000 rpm at a constant temperature of 20.0  $^\circ\text{C}$ . Concentration profiles and the movement of the sedimenting boundary in the analytical ultracentrifuge cell were recorded using the Rayleigh interference optical system. The data were then analyzed using both the time derivative  $g(s^*)$  and Lamm Equation fitting software in SEDANAL [48] (<http://sedanal.bbri.org/>). The  $s_{T,b}^*$  value of the principal component in each  $g(s^*)$  vs.  $s_{T,b}^*$  plot, where the \* indicates that the distribution of sedimentation coefficients has not been corrected for diffusion effects [49], was then determined with PeakFit by fitting the data with a series of Gaussians.

As sedimentation coefficients are temperature and solvent dependent, it is conventional to convert them (or their distributions) to the standard conditions of 20.0  $^\circ\text{C}$  and water using the following equation [50]:

$$s_{20,w} = s_{T,b}^* \left[ \frac{(1 - \bar{v}\rho_{20,w})\eta_{T,b}}{(1 - \bar{v}\rho_{T,b})\eta_{20,w}} \right] \quad (1)$$

where  $\bar{v} = 0.715$ , 0.719, and 0.716  $\text{ml g}^{-1}$  are the partial specific volumes of hHMW-FG, hFrX, and cFG, respectively (computed by PRO-MOLP [40]; see Section Characterization of fibrinogen and fragment X samples),  $\eta_{T,b}$  and  $\rho_{T,b}$  are the viscosity and density of the solvent (TBS) at the experimental temperature (20.0  $^\circ\text{C}$ ), 1.0242 cP and 1.0004  $\text{g ml}^{-1}$ , respectively, and  $\eta_{20,w}$  and  $\rho_{20,w}$  are the viscosity and density of water at 20.0  $^\circ\text{C}$ .

To account for hydrodynamic non-ideality (co-exclusion and backflow effects), the apparent sedimentation coefficients ( $s_{20,w}$ ) were calculated at each concentration and extrapolated to infinite dilution ( $s_{20,w}^0$ ) using the following equation [50–52].

$$(s_{20,w})^{-1} = (s_{20,w}^0)^{-1} (1 + k'_s c) \quad (2)$$

where  $k'_s$  ( $\text{ml g}^{-1}$ ) is the apparent sedimentation concentration dependence or “Gralén” coefficient [51]. When the data from a series of loading concentrations were globally fit with SEDANAL, Eq. (2) was included in the fitting model to determine the true  $k_s$ , while the second virial coefficient  $BM1$  was accounted for in the diffusion term [53]:

$$D_{t(20,w)} = D_{t(20,w)}^0 (1 + 2BM1c)(1 + k_s c)^{-1} \quad (3)$$

A non-ideal self-associating monomer–dimer single-component model was used in the global fitting [53].

#### Size-exclusion high-performance liquid chromatography (SE-HPLC) coupled to multi-angle laser light scattering (MALLS) and differential pressure viscometry (DPV)

Analytical fractionation was carried out using two SE 7.8  $\times$  300 mm columns (TSK G4000PW and G3000PW, Tosoh Bioscience, Tokyo, Japan; <http://www.tosohbioscience.com/>) connected in series, protected by a similarly packed 6  $\times$  40 mm guard column. Chromatograms were acquired on-line with UV (Cecil 1100 series, Cambridge, UK), MALLS (DAWN HELEOS II, Wyatt Technology, Santa Barbara, CA; <http://www.wyatt.com/>), DPV (Viscostar II, Wyatt Technology) and differential refractive index (Optilab rEX, Wyatt Technology) sequentially placed detectors. The eluent (TBS) was pumped at 0.8  $\text{ml min}^{-1}$  (PU-1580, Jasco Corporation, Great Dunmow, UK; <http://www.jascoinc.com/>), and the samples were manually injected using a Beckman Altex 210A valve with a 500  $\mu\text{l}$  PEEK loop. Samples were centrifuged for 5 min at 10,000g before injection, and a 0.1  $\mu\text{m}$  on-line filter was placed right after the columns to reduce particulate and improve the MALLS detectors' signal-to-noise ratio. The runs were made at room temperature ( $\sim 28$   $^\circ\text{C}$ ), with no thermostating of the columns and of the UV and MALLS cells (K5 type); the temperature of the latter was monitored and recorded by the ASTRA<sup>®</sup> (Version 5.3.2.17) collection and analysis software (Wyatt Technology) controlling the DAWN HELEOS II, Viscostar II, and Optilab rEX instruments. The DPV capillaries and RI cell were instead kept at 20.0  $^\circ\text{C}$ .

Absolute rms z-average radii of gyration ( $\langle R_g^2 \rangle_z^{1/2}$ ), weight-average molar masses ( $\langle M \rangle_w$ ), and weight-average intrinsic viscosities ( $\langle [\eta] \rangle_w$ ) were calculated using the ASTRA<sup>®</sup> software. The MALLS was factory calibrated with toluene, using a Rayleigh ratio of  $4.1159 \times 10^{-5} \text{ cm}^{-1}$  at 25  $^\circ\text{C}$  and at a wavelength of 658 nm. The refractive index of the TBS solvent was 1.334 at 20  $^\circ\text{C}$  at 633 nm, as previously determined [54], and used as such. Both the reference Rayleigh ratio and solvent refractive index are automatically corrected to the actual (measured) temperature by the ASTRA software. The normalization procedure of the DAWN photodiodes was done by injecting an 11 mg/ml bovine serum albumin (BSA) solution in TBS in the SE-HPLC system and selecting a narrow region of the main eluting peak. A rms  $R_g$  of 3 nm was used in the normalization, and the resulting  $\langle M \rangle_w$  of the peak slices, using  $dn/dc = 0.1866 \text{ ml g}^{-1}$  (extrapolated

at the  $\lambda = 658$  nm of the DAWN HELEOS II laser from literature data at  $\lambda = 436$  and  $546$  nm [55]) and RI detection, was 65,200, in very good agreement with the value determined from the BSA composition, 66,283. Literature experimental values of the refractive index increment,  $dn/dc$ , are available only for unfractionated FG at lower wavelengths [56], and yielded a value of  $0.191 \text{ ml g}^{-1}$  by interpolation at  $658$  nm. This value was then used in the calculation of  $\langle M \rangle_w$  for hHMW-FG and cFG. For hFrX, a value of  $0.193 \text{ ml g}^{-1}$  was used, based on comparisons between theoretical calculations of  $dn/dc$  for all the three species [57–59] using PROMOLP [40], which, however, gave much smaller values not compatible with the experimental evidence. The concentration of each peak slice was determined from the UV detector signal for the hHMW-FG and hFrX samples, using extinction coefficients of  $1.53 \times 10^{-3}$  and  $1.69 \times 10^{-3} \text{ ml g}^{-1}$ , respectively, calculated by PROMOLP [40] from their composition (see Results and discussion). For hHMW-FG, the computed value is very close to the experimental extinction coefficient measured on unfractionated hFG,  $1.51 \text{ ml g}^{-1}$  [39]. For cFG, the concentration was determined by the RI detector, using a  $dn/dc$  of  $0.191 \text{ ml g}^{-1}$ .

## Results and discussion

### Characterization of fibrinogen and fragment X samples

A typical final purification step by SEC of the plasmin digestion products of the hLMW'-FG fraction is reported in Fig. 2, where the chromatogram and the SDS-urea-PAGE analysis of some unreduced fractions are reported. As can be seen both from its shape and from the SDS-urea-PAGE analysis, the main peak contains two components, and it's possible to separate the first (fractions 1–2) from its mixture with the second (fractions 3–6). The other peaks contain more degraded (7–8) or other (9) unwanted material, and are discarded (note that, due to the non-reduction of the samples, the molecular weight of the standards are to be taken only as purely indicative). Fractions 1–2 were therefore kept, and after concentration and re-chromatography of the pool made with fractions 3–6, a good yield of practically monodisperse hFrX could be obtained.

In Fig. 3 we report the analysis by SDS-urea-PAGE of starting materials and typical preparations of our purified samples. As can be seen, the samples (lanes 3, 4, 7, 8) appear to be reasonably monodisperse by this criterion; cFG (lane 4) and one hFrX preparation (lane 7) show traces of higher molecular weight contaminants.

A further characterization step was taken on reduced samples, as shown in Fig. 4. To reliably quantify the relative proportion of each species within a particular sample, various loads were applied. In the 12.5% T SDS-PAGE gel on the left side panel, the hHMW-FG samples show only the typical triplet of bands corresponding to the  $\text{A}\alpha$ ,  $\text{B}\beta$ , and  $\gamma$  chains, respectively, with the  $\text{A}\alpha$  band split in two. However, it is well known that the early C-terminal degradation products of this chain have molecular weights very close to those of the  $\text{B}\beta$  and  $\gamma$  chains, thus co-migrating with them (see [44]). Therefore, a Western blot analysis, using the Y18 MAb specific for the N-terminal of the  $\text{A}\alpha$  chain [42], was performed. The results, shown on the center and center-right panels in Fig. 4, demonstrate that bands corresponding to some  $\text{A}\alpha$  chain C-terminal early degradation products become visible only at the highest loading concentrations (first two lanes of the center panel). Western blot analysis using the J88B MAb specific for the  $\gamma$  chain [43] confirmed the presence of a single band (Fig. 4, right-side panel). As for hFrX, the Coomassie Blue stain (Fig. 4, left panel) evidenced a major band at the position of the  $\gamma$  chain, and a doublet of fainter bands migrating between the 31 and 21.5 K markers bands. In addition, another fainter band migrates just be-

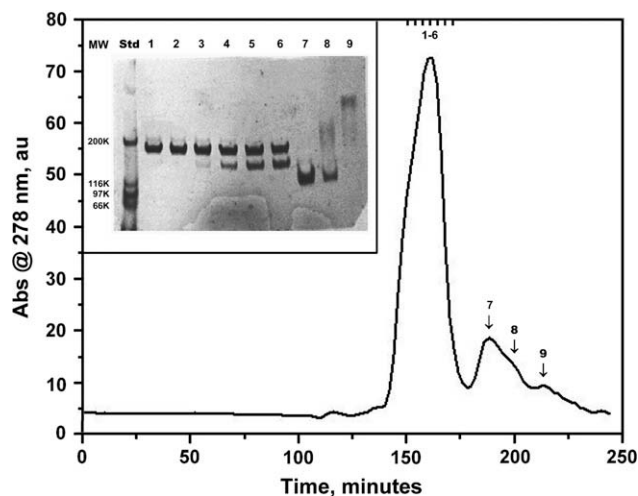


Fig. 2. SEC purification of hFrX. Typical separation of plasmin digestion products on the Superdex 200 Prep Grade column. The fractions indicated on the upper x axis and by the arrows in the main panel were analyzed unreduced by SDS-urea-PAGE on 3.2% T PAA gels, as shown in the inset (note that the total protein concentration loaded is the same for each well); the molecular weight of the standards (Std.) are indicated on the left side.

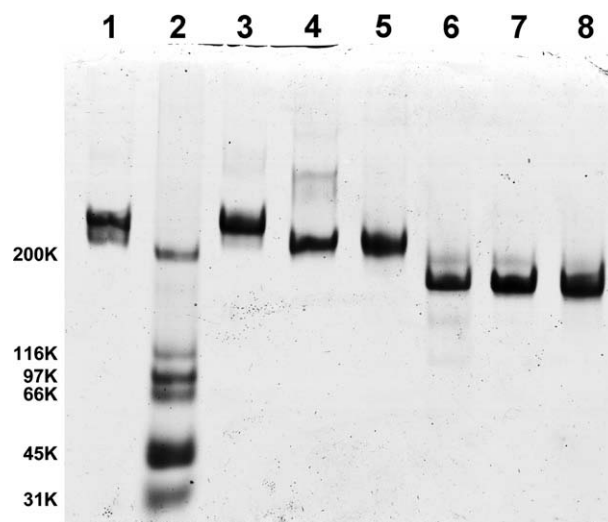
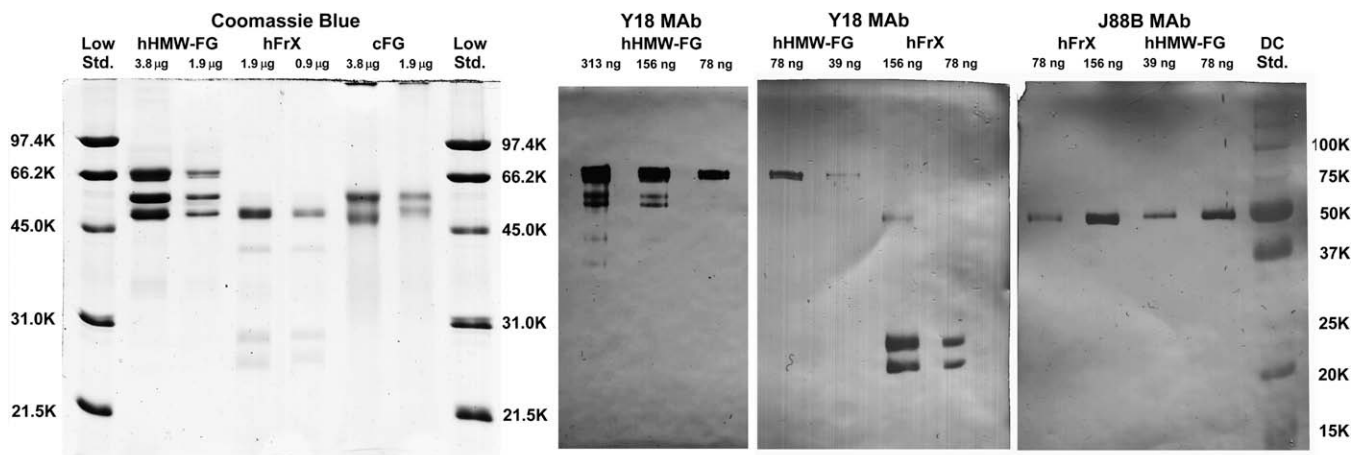


Fig. 3. SDS-urea-PAGE analysis of various FG unreduced samples on a 3.2% T PAA gel. Lane 1, FG starting material; lane 2, Bio-Rad Broad molecular weight standard; lane 3, hHMW-FG; lane 4, cFG; lane 5, hLMW'-FG; lane 6, plasmin digest of hLMW'-FG before SE-FPLC; lanes 7 and 8, two different hFrX preparations after SE-FPLC. Samples loads were all  $1.9 \mu\text{g}$ ,  $15 \mu\text{l}$ .

low the 45 K marker. The presence of a single major band indicates that the ( $\text{B}\beta$ ) chain has most likely lost the first  $\sim 50$  N-terminal residues during plasmin digestion [27], thus co-migrating with the  $\gamma$  chain. The Western blot analysis with the Y18 MAb (Fig. 4, rightmost two lanes on the center-right panel) confirmed that the two lower bands were C-terminally degraded  $\text{A}\alpha$  chains, and showed a higher molecular weight  $\text{A}\alpha$  chain contaminant only at the higher loading concentration. The J88B staining instead confirmed the near-intactness of the  $\gamma$  chains (Fig. 4, leftmost two lanes in the right-side panel), which might have therefore lost only the 407–411 C-terminal residues (see [60]).

The identity of the bands in the hFrX preparations was then further checked with PMF (by AP/MALDI-TOF MS, see Materials and methods, Protein characterization by mass spectrometry). This



**Fig. 4.** SDS-PAGE and Western blot analysis of reduced FG samples. Left panel: 12.5% T SDS-PAGE with Coomassie Blue staining of hHMW-FG, hFrX, and cFG samples, with the total amount loaded indicated (sample volumes were all 15  $\mu$ l); the two outermost lanes contained Bio-Rad's low molecular weight unstained standards (Low Std.), with their masses indicated. Other panels: Western blots from 12% T PAA gels of hHMW-FG and hFrX samples immunostained with the Y18 MAb against the  $A\alpha$  chain N-terminus (center and center-right panels) and with the J88B MAb against the  $\gamma$  chain 63–70 segment (right panel; the last lane contains Bio-Rad's Dual-color molecular weight standards, DC Std.). Total amounts loaded as indicated, sample volumes were all 2.5  $\mu$ l.

confirmed with high confidence that the major band migrating just above the 45 K marker in Fig. 4, left panel, contains both  $\beta$  and  $\gamma$  chain species, with traces of an ( $A$ ) $\alpha$  chain remnant just above it, and that the two less colored bands between the 21.5 K and 31.0 K markers belong to ( $A$ ) $\alpha$  chain degradation products. Furthermore, we identified the fainter band visible just below the 45 K marker as deriving from the  $\beta$  chain, while another couple of lower molecular weight bands (not visible in Fig. 4), contained  $\gamma$  chain peptides (also confirmed by Western blotting with the J88B MAb on overloaded gels; data not shown). These results suggest that while the bulk of the preparation contained relatively monodisperse, intact hFrX, there were some additional cuts in the  $\beta$ - and/or  $\gamma$  chains in a minority of the molecules, which were not released from the main body because of disulfide bridges and other structural constraints. We unsuccessfully tried to determine the true molecular weight of these bands directly excised from the gels and examined by RP-HPLC-ESI-TOF MS, likely because we could not remove the remaining SDS. From a rough estimate with the SDS-PAGE molecular weight standards, their masses are  $\sim$ 43,000 and  $\sim$ 39,000, respectively. For the  $\beta$  chain band, this would correspond to a  $\beta$ 123–461 fragment, deriving from a cut in the middle of the coiled-coil region (see [60]). For the  $\gamma$  chain, the putative fragment could be  $\gamma$ 63–406, still bearing the J88B epitope [43], with the cut again positioned in the middle of the coiled-coil (see [60]). The N-terminal segments derived from these cuts, with putative masses of  $\sim$ 7450 and  $\sim$ 9300, respectively, likely eluted from the bottom of our gels. These results are fully consistent with the known pathway of FG degradation producing fragment Y and fragment D from fragment X by cuts in the middle of the coiled-coil region, and are an almost unavoidable product of bulk plasmin digestion [60]. Fortunately, under our conditions these byproducts appear to have been contained to a minimum.

The molecular masses of the  $A\alpha$ ,  $B\beta$ ,  $\beta$ , and  $\gamma$  chains in hHMW-FG and hFrX were then determined by RP-HPLC-ESI-TOF MS starting from reduced samples without prior separation by SDS-PAGE (see Materials and methods, Protein characterization by mass spectrometry). In Fig. 5, the % total ion current (TIC) vs. elution time raw chromatograms are reported for reduced hHMW-FG (panel A) and hFrX (panel B). The assignment of the peaks to the FG chains, as indicated in the figure, was made on the basis on the known elution behavior of hFG chains under similar conditions [61], later confirmed by comparing the measured masses with those calculated from the sequences (see below). The gray boxes

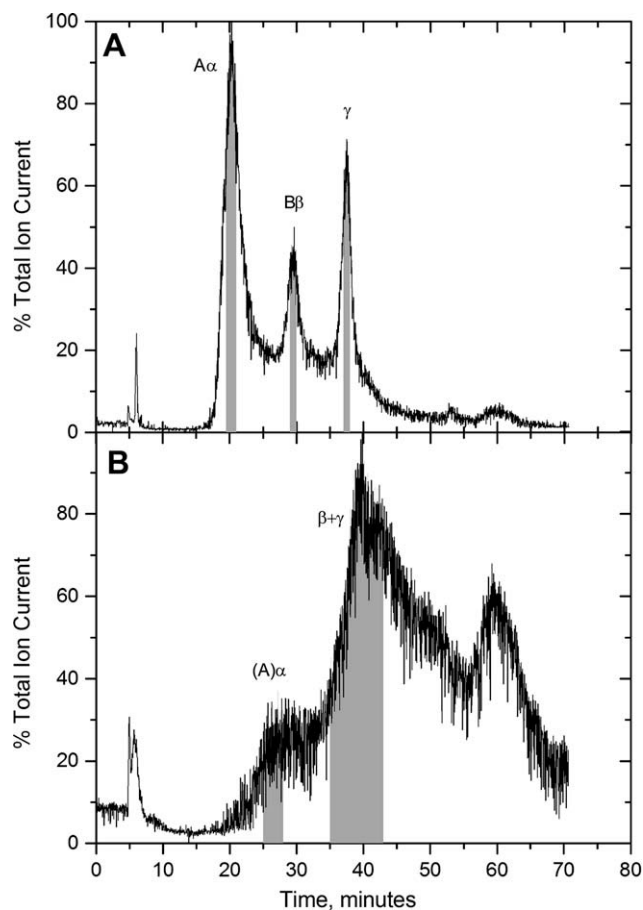


**Fig. 5.** % Total ion current (TIC) vs. elution time RP-HPLC-ESI-TOF MS chromatograms for reduced hHMW-FG (panel A) and hFrX (panel B). The gray-shaded areas correspond to the zones that were selected for further analysis, with the assignment to the various chains indicated.

indicate the portion of the chromatograms that were converted first into raw abundance vs.  $m/z$  mass spectra, and then deconvoluted in order to obtain the actual protein masses. As an example, the raw abundance vs.  $m/z$  spectra derived from the boxed areas of the peaks in Fig. 5, panel A, corresponding to the  $A\alpha$ ,  $B\beta$ , and  $\gamma$  chains,

are reported in Fig. 6. The deconvoluted spectra are shown in Fig. 7, where all the processed peaks are numbered, with their masses reported in Table 1.

As can be seen in Table 1, we have positively retrieved all the major forms of the chains derived from hHMW-FG (peaks 1–4, 6–8, 9–10). A higher molecular weight minor component of the A $\alpha$  chains pool is also present (peak 5), which we have tentatively identified as a partially processed form, A $\alpha$ 1–618 (without post-translational phosphorylation), while peak 6 could be a C-terminal degradation product of the B $\beta$  chain. As for hFrX, the data in Table 1 establish that the A $\alpha$  chain remnants are A $\alpha$ 1–206 and A $\alpha$ 1–219 (peaks 11–12), and confirm the presence of some less degraded species (peaks 13–15). The  $\gamma$  chains appear to be mostly intact, although the  $\gamma$  1–406 form is compatible with the data, but both are nearly indistinguishable from B $\beta$  chains that have lost the first ~53 N-terminal residues, the form  $\beta$ 54–461 being predominant (peaks 16–18). In addition, both  $\beta$  and  $\gamma$  chains can have one or two terminal sialic acids present on their carbohydrate moieties (as in peaks 7–8 and 9–10), further complicating the analysis. The  $\gamma$  chain intermediate cut band (MW ~39,000 from SDS-PAGE) was also found re-analyzing the MS data of Fig. 5, panel B (MW 36,257, data not shown), establishing its identity as likely  $\gamma$ 86–406 (MW 36,417). However, we could not find any trace of the corresponding  $\beta$  chain MW ~43,000 band, perhaps due to poor solubility in our HPLC solvent system.

The values in the last column of Table 1 are the relative percentages of the species determined from the densitometric analysis of the Western blots stained with the Y18 MAb presented in Fig. 4. Combining together these data, we could compute the most likely values for the molecular weight, partial specific volume, and extinction coefficient of the hHMW-FG and hFrX species whose solution properties were then studied (see below). Those values are reported in Table 2, together with those of cFG computed from its putative composition.

#### Analytical ultracentrifugation

The results of the SEDANAL ( $g(s^*)$ ) vs.  $s_{T,b}^*$  analyses for the hHMW-FG, cFG, and hFrX samples and their fitting with Gaussian

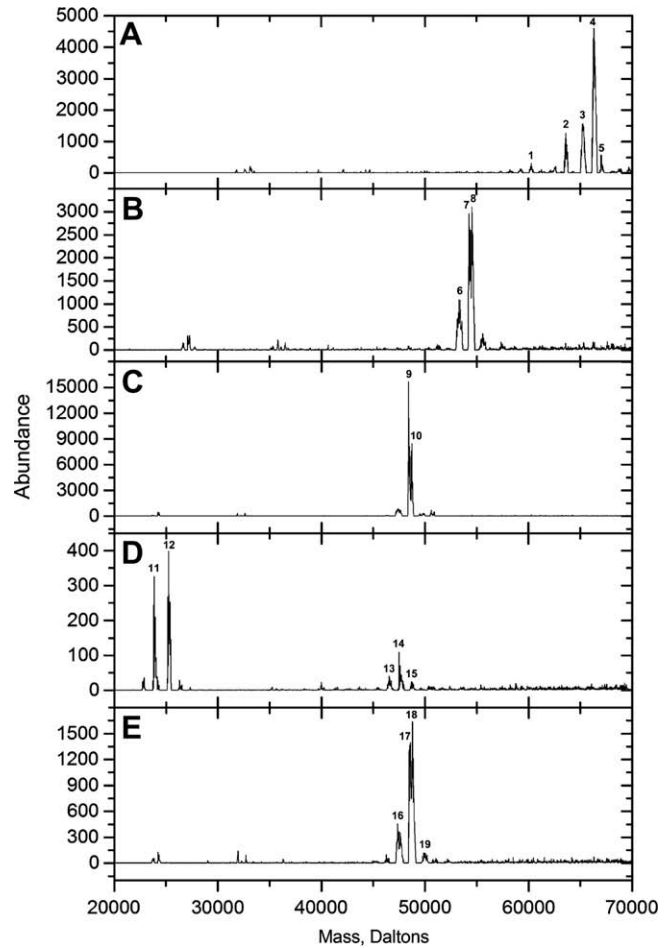


**Fig. 7.** Deconvoluted mass spectra derived from the % TIC vs. elution time boxed regions in Fig. 5. Panel A, hHMW-FG A $\alpha$  chain; panel B, hHMW-FG B $\beta$  chain; panel C, hHMW-FG  $\gamma$  chain; panel D, hFrX (A) $\alpha$  chain; panel E, hFrX  $\beta$  +  $\gamma$  chains. For the identification and mass values of the numbered peaks, see Table 1.

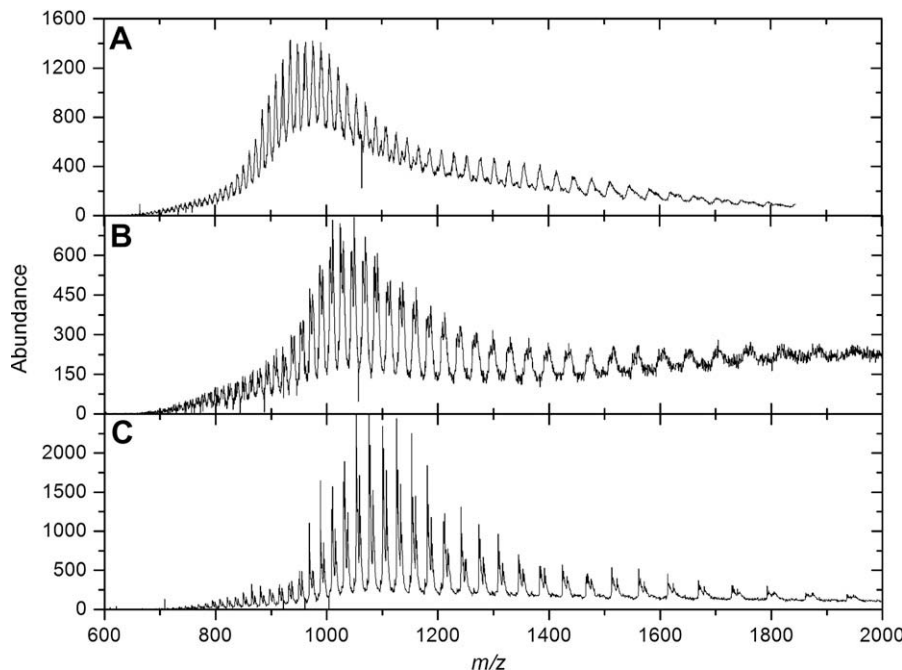


**Fig. 6.** Raw abundance vs.  $m/z$  ratios spectra obtained from the boxed regions of the three peaks in Fig. 5, panel A. Panel A, A $\alpha$  chain; panel B, B $\beta$  chain; panel C,  $\gamma$  chain.

**Table 1**

Mass values of the labeled peaks in Fig. 7, with their identification, comparison with calculated masses based on the protein composition, and other computed properties. In the last column are reported the relative % derived from the densitometric analysis of Western blots.

Peak #	Mass from MS	Identification	Mass from composition	$E^{280}$ (ml mg <sup>-1</sup> cm <sup>-1</sup> )	$\bar{v}$ (ml g <sup>-1</sup> )	Relative % (from gels)
1	60,087	A $\alpha$ 1-554	60,022	1.07	0.713	3.6
2	63,489	A $\alpha$ 1-583	63,250	1.09	0.712	3.4
3	65,056	A $\alpha$ 1-601	65,105	1.06	0.711	30.5
4	66,134	A $\alpha$ 1-610	66,094	1.04	0.711	62.5
5	66,942	A $\alpha$ 1-618 (no P)?	(66,956)	(1.03)	(0.711)	-
6	53,070	B $\beta$ 1-449 (SIA <sub>2</sub> )?	(52,975)	(1.95)	(0.714)	-
7	54,211	B $\beta$ 1-461 (SIA <sub>1</sub> )	54,175	1.91	0.716	-
8	54,503	B $\beta$ 1-461 (SIA <sub>2</sub> )	54,467	1.90	0.715	-
9	48,385	$\gamma$ 1-411 (SIA <sub>1</sub> )	48,373	1.77	0.720	-
10	48,676	$\gamma$ 1-411 (SIA <sub>2</sub> )	48,665	1.76	0.720	-
11	23,746	A $\alpha$ 1-206	23,830	0.73	0.725	46.8
12	25,169	A $\alpha$ 1-219	25,254	0.69	0.728	47.2
13	46,361	A $\alpha$ 1-424	46,223	1.39	0.712	6.0
14	47,491	A $\alpha$ 1-439	47,758	1.35	0.712	-
15	48,602	A $\alpha$ 1-448	48,748	1.32	0.712	-
16	47,172	$\beta$ 54-449 (SIA <sub>2</sub> )?	(47,325)	(2.15)	(0.714)	-
17	48,420	$\beta$ 54-461 (SIA <sub>1</sub> )	48,525	2.10	0.715	-
		$\gamma$ 1-411 (SIA <sub>1</sub> )	48,373	1.77	0.720	-
		$\gamma$ 1-406 (SIA <sub>2</sub> )	48,194	1.77	0.720	-
18	48,707	$\beta$ 54-461 (SIA <sub>2</sub> )	48,817	2.09	0.715	-
		$\gamma$ 1-411 (SIA <sub>2</sub> )	48,665	1.76	0.720	-
19	49,701	$\beta$ 43-461 (SIA <sub>1</sub> )?	49,620	2.05	0.716	-

**Table 2**

Calculated molecular properties of the hFrX, cFG, and hHMW-FG species.

Species	Molecular weight (g mol <sup>-1</sup> )	$\bar{v}$ (ml g <sup>-1</sup> )	$E^{280}$ (ml mg <sup>-1</sup> cm <sup>-1</sup> )
hFrX	245,600	0.719	1.69
cFG	320,734 <sup>a</sup>	0.716 <sup>a</sup>	1.34 <sup>a</sup>
hHMW-FG	336,634	0.715	1.53

<sup>a</sup> Values derived only from the theoretical composition.

curves are reported in the Electronic Supplementary material (Supplementary Figs. 1–3). For hHMW-FG, a single major peak was found in each sample except that at  $c = 0.482$  mg ml<sup>-1</sup> (Supplementary Fig. 1). A similar situation holds also for the hFrX samples (Supplementary Fig. 3), where only the  $c = 0.673$  mg ml<sup>-1</sup> run shows a second major component; however, there were hints of two closely-related species, that we did not attempt to separate, in at least two other samples ( $c = 0.446$  and  $c = 1.488$  mg ml<sup>-1</sup>). As for cFG, the samples were more heterogeneous, requiring two additional relevant components besides the major one (Supplementary Fig. 2). The  $s_{T,b}^*$  peak values of the main components were then reduced to standard conditions ( $s_{20,w}$ ), and their inverse are reported in Fig. 8 as a function of the loading concentration. For the cFG and hHMW-FG samples, the  $\langle s_{20,w}^0 \rangle_w$  values extrapolated by weighted linear regression from each data set are collected in Table 3. The apparent hydrodynamic concentration constants  $k'_s$  derived from the  $\langle s_{20,w} \rangle_w^{-1}$  vs.  $c$  plots for all samples are also reported in Table 3. Since the slightly negative  $k'_s$  for hFrX was indicative of moderate self-association, the best-quality four datasets were then globally fitted with a non-ideal, self-associating monomer-dimer single-component model (see Supplementary Fig. 4). From this fit, the translational diffusion coefficient  $\langle D_{t(20,w)}^0 \rangle_z$  was also recovered, from which the monomer weight-average molecular weight ( $M_w$ ) could then be calculated using the Svedberg equation (Table 3). Furthermore, the global fit provided an estimate of the true hydrodynamic concentration constant  $k_s$  ( $59.3 \pm 18.1$  ml g<sup>-1</sup>) and of the second virial coefficient  $BM1$  ( $217 \pm 117$  ml g<sup>-1</sup>) for hFrX. In addition, Table 3 includes the molecular weight ( $M_w$ ) computed for hHMW-FG via the Svedberg equation, utilizing a literature  $\langle D_{t(20,w)}^0 \rangle_z$  value [62,63]. Examining in detail the data of Fig. 8 and Table 3, the positive  $k'_s$  for both

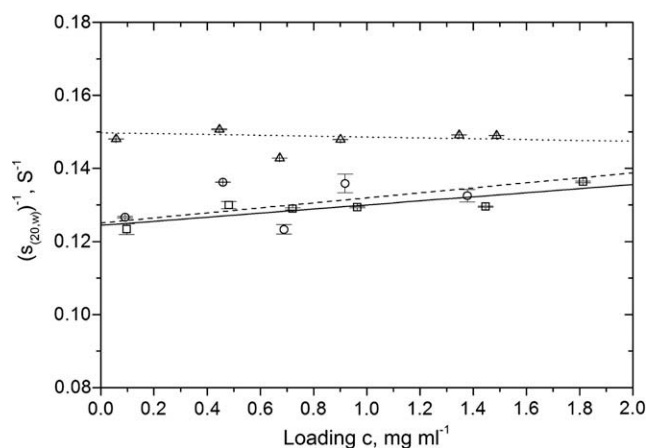


**Fig. 8.** Concentration dependence of the reciprocal of the experimental sedimentation coefficients  $\langle s_{20,w}^0 \rangle_w^{-1}$ , extracted from Gaussian fits of the  $\langle g(s^*) \rangle$  vs.  $s_{T,b}^*$  plots and corrected to standard conditions, and their linear regression analysis for hHMW-FG (open squares, solid line), cFG (open circles, dashed line), and hFrX (open triangles, dotted line).

hHMW-FG and cFG are in agreement with previous reports of AUC data for hFG [26,64]. The extrapolated  $\langle s_{20,w}^0 \rangle_w$  value for hHMW-FG is a bit higher than the traditionally accepted value of 7.8–7.9 S [4,65], although it should be pointed out that these literature data are averages taken from an earlier compilation [66], where the experimental data spread is quite large. This is not surprising given the susceptibility of fibrinogen (and fragment X) to aggregation and degradation, coupled with the less refined characterization of the samples in those earlier reports. In any case, the molecular weight calculated from our hHMW-FG  $\langle s_{20,w}^0 \rangle_w$  value and the literature  $\langle D_{t(20,w)}^0 \rangle_z$  data for human FG, reported in Table 3, is in excellent agreement with the composition of our sample determined by MS and SDS-PAGE/Western blot analyses (Table 2). As for cFG, no literature data are available on its hydrodynamic properties, to the best of our knowledge. Therefore, we can only point out that the  $\langle s_{20,w}^0 \rangle_w$  value is practically indistinguishable from that of the hHMW-FG sample, although there is a larger uncertainty ( $\sim 7\%$  vs.  $\sim 2\%$ ). After factoring in the relative molecular

**Table 3**  
Parameters derived from the SEDANAL analysis of the sedimentation velocity data for hFrX (global fit, non-ideal self-associating monomer–dimer single-component model), and for cFG and hHMW-FG (linear regression of Gaussian fits of  $\langle g(s^*) \rangle$  vs.  $s_{T,B}^*$  plots).

Sample	$\langle s_{(20,w)}^0 \rangle_w$ (S)	$\langle D_{t(20,w)}^0 \rangle_z$ (F)	$\langle M \rangle_w$ (% diff.) <sup>a</sup> (g mol <sup>-1</sup> )	$k'_s$ <sup>b</sup> ( $\pm$ SD) (ml g <sup>-1</sup> )	Fit SD
hFrX	6.83 <sup>c</sup> $\pm$ 0.06 <sup>d</sup>	2.52 <sup>c</sup> $\pm$ 0.15 <sup>d</sup>	234,219 <sup>e</sup> $\pm$ 13,968 <sup>d</sup> (-5%)	-7.8 $\pm$ 0.5	0.02 <sup>c</sup>
cFG	8.00 <sup>b</sup> $\pm$ 0.53 <sup>f</sup>	nd	na	54.9 $\pm$ 65.6	0.006 <sup>b</sup>
hHMW-FG	8.04 <sup>b</sup> $\pm$ 0.12 <sup>f</sup>	2.0 <sup>g</sup>	342,261 <sup>e</sup> (+2%)	44.9 $\pm$ 13.6	0.002 <sup>b</sup>

<sup>a</sup> % Difference from mass spectrometry- and SDS-PAGE/Western blot-derived values (see Table 2).

<sup>b</sup> From the weighted linear regression fit of the  $\langle s_{(20,w)} \rangle^{-1}$  vs.  $c$  plots.

<sup>c</sup> From the global fit.

<sup>d</sup> Approximated SD derived from the 95% confidence limits as half of the mean of the differences from the mean value.

<sup>e</sup> Calculated from the  $\langle s_{(20,w)}^0 \rangle_w$  and  $\langle D_{t(20,w)}^0 \rangle_z$  values using the Svedberg equation ( $\bar{v}$  from Table 2).

<sup>f</sup> SD.

<sup>g</sup> Literature value [62,63].

weights and  $\bar{v}$  (Table 2), the Stokes' radii  $R_s$  computed from the  $\langle s_{(20,w)}^0 \rangle_w$  values differ by  $\sim 4\%$  (10.5 vs. 10.1 nm, respectively). This suggests that the presence/absence of the 11/12 repeats in the middle of the  $\alpha C$  regions (see Fig. 1) has only a relatively minor effect on the hydrodynamic behavior of fibrinogen. Instead, hFrX has sensibly lower  $\langle s_{(20,w)}^0 \rangle_w$  and higher  $\langle D_{t(20,w)}^0 \rangle_z$  values, which translates into a  $R_s$  of  $\sim 8.5$  nm ( $\sim -20\%$ ), suggesting a larger overall shape change upon removal of the  $\alpha C$  regions. Compared with the available literature data [26], our hFrX value is slightly lower (6.8 vs. 7.0 S), while the  $\langle D_{t(20,w)}^0 \rangle_z$  value is nearly identical to that previously reported [62]. Taken together, this justifies also the somewhat lower  $\langle M \rangle_w$  ( $\sim -5\%$ ) in respect with the composition

data (see Table 2). Interestingly, the lower  $k'_s$  value for hFrX, coupled with its positive  $BM1$  value, suggests that removal of the  $\alpha C$  regions alters the solute–solute interactions of FG allowing limited dimerization ( $K_{eq} \approx 1.1 \times 10^4$ ).

#### SE-HPLC–MALS–DPV

In Fig. 9 are reported the chromatographic profiles from the SE-HPLC–MALS–DPV set-up for the three samples investigated, hFrX (panel A), cFG (panel B) and hHMW-FG (panel C). The black and blue traces are from the two concentration detectors used, (UV and RI, respectively), while the red and green traces are from the 90° scattering angle of the MALS and from the DPV detectors, respectively. In each panel, the traces have been re-aligned on the time scale to account for the delays due to the sequential position of the detectors (UV–MALS–DPV–RI), and the voltages were also arbitrarily rescaled. However, the relative proportions of the UV and 90° MALS detectors have been preserved in each panel. The elution times of each major peak are indicative of the hydrodynamic dimensions of the species, and it can be immediately seen that while hFrX elutes later (Fig. 9, panel A), there are practically no differences between cFG and hHMW-FG (Fig. 9, panels B and C). Starting from hFrX (Fig. 9, panel A) and examining the traces in more details, it is evident the total absence of any aggregates and intact fibrinogen signals, and the peak is only slightly skewed toward the right side, indicating a low degree of polydispersity.

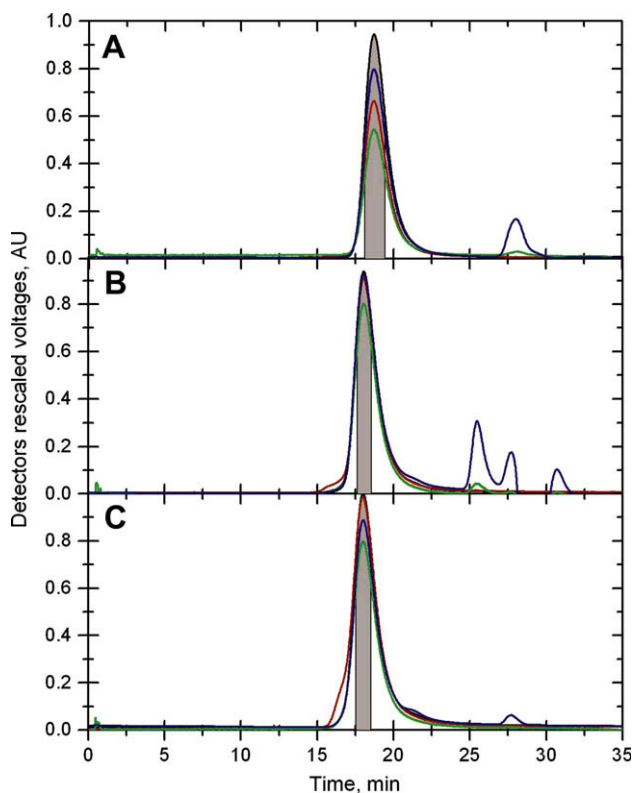


**Fig. 9.** Elution profiles from SE-HPLC with UV (black), light scattering at 90° (red), DPV (green) and RI (blue) detection for hFrX (panel A), cFG (panel B) and hHMW-FG (panel C). In each panel, the intensities have been arbitrarily rescaled to render each signal fully visible, but trying to preserve the relative proportion between the concentration detectors and the scattering detector. The gray areas are the peak limits utilized for computing the  $\langle (R_g^2)_z \rangle^{1/2}$ ,  $\langle M \rangle_w$  and  $\langle [\eta] \rangle_w$  of the species under consideration. The injection volumes and samples concentration were 150  $\mu$ l at 5.0 mg/ml for hFrX, 100  $\mu$ l at 8.3 mg/ml for cFG, and 100  $\mu$ l at 9.15 mg/ml for hHMW-FG.

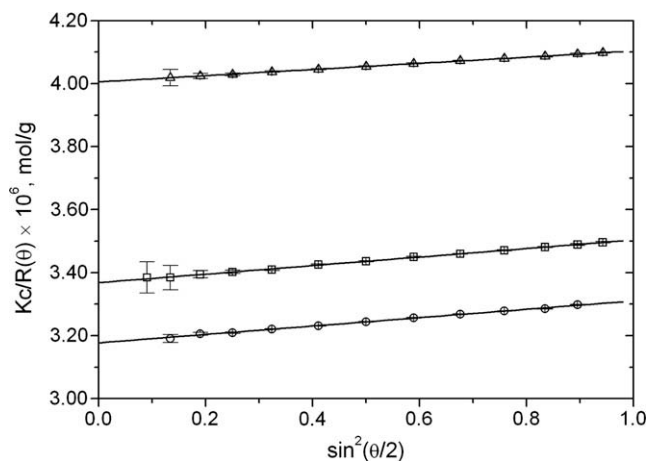


**Fig. 10.** Zimm plots of the data from the MALS and concentration detectors for the top peak SE-HPLC slices of the Fig. 9 chromatograms for hFrX (triangles), cFG (circles), and hHMW-FG (squares). The straight lines are the linear regressions from which the molecular weight and mean square radius of gyration are derived. The individual error bars on each point factor in the detector noise, established at baseline, and the  $\chi^2$  of the fit.

**Table 4**

Parameters derived from the SE-HPLC–MALLS–DPV analysis of hFrX, cFG, and hHMW-FG.

Sample	Peak top (min)	Peak limits (min)	$\langle M \rangle_w$ (% diff.) <sup>a</sup> (g mol <sup>-1</sup> )	$(\langle R_g^2 \rangle_z)^{1/2}$ (nm)	$\langle [\eta] \rangle_w$ (cm <sup>3</sup> g <sup>-1</sup> )	$R_E$ (nm)
hFrX	18.71	18.27–19.12	250,000 ± 250 (+2%)	11.3 ± 0.4	20.7 ± 0.06	9.4
cFG	18.05	17.62–18.55	298,500 ± 300 (-7%)	13.7 ± 0.1	26.9 ± 0.08	10.8
hHMW-FG	18.00	17.55–18.50	334,400 ± 300 (-1%)	14.1 ± 0.1	27.3 ± 0.08	11.3

<sup>a</sup> % Difference from mass spectrometry- and SDS–PAGE/Western blot-derived values (hFrX and hHMW-FG), and from composition-derived values (cFG) (see Table 2).

The small peak at ~28 min visible only in the RI and DPV traces is most likely due to buffer components present in the injected sample. This hypothesis is confirmed by the observation of even more evident later-eluting “peaks” in the RI and DPV traces of cFG (Fig. 9, panel B), which was originally stored in a buffer different from that used in our SE-HPLC experiments. Still examining the cFG elution profile, we notice a slight amount of aggregates eluting just in front of the main peak, and some degradation products eluting after it. In any case, the main peak boundaries chosen for the analysis (shaded gray area) should exclude any influence of these species in the calculations. A slightly higher proportion of aggregates is present in the hHMW-FG sample (Fig. 9, panel C), also followed by some degradation products. As in the cFG case, we have tried to avoid as much as possible their influence on the parameters’ computation by choosing appropriate main peak boundaries.

In Fig. 10 three Zimm plots, generated from the MALLS and concentration detectors signals for the top peak slices of hFrX (triangles), cFG (circles), and hHMW-FG (squares), are reported. The MALLS detectors used, with their corresponding scattering angles within brackets, were 6–17 (42.9–152.2°) for hFrX, 5–17 (35.0–152.2°) for cFG, and 6–16 (42.9–142.3°) for hHMW-FG. These settings were chosen after visual examination of the Zimm plots of all the slices included in the analysis (gray-shaded areas inside the peaks in Fig. 9), the signal from the other available detectors being excluded because too noisy or inconsistent. Considering that the dimensions of the FG species under consideration are at the very limit of detection for angular dependence of the scattered light for the incident wavelength used (658 nm), the Zimm plots in Fig. 10 appear to be rather good.

The full set of parameters derived from the SE-HPLC–MALLS–DPV data are reported in Table 4. It must be pointed out that the data computed by the ASTRA<sup>®</sup> software are averages taken over all the slices included in the peaks, and their associated uncertainties are only statistical, not including any systematic error that might be present (for instance, errors in  $dn/dc$ , extinction coefficients or calibration/normalization constants). With these caveats, we can immediately notice the excellent agreement between the MALLS-derived  $\langle M \rangle_w$  reported in Table 4 for hFrX and hHMW-FG, and those determined by the SDS–PAGE/Western blot/MS analysis, 246,000 and 337,000, respectively (see Table 2). This agreement indicates that we are indeed analyzing nearly-monodisperse samples, and that we are likely determining the slices’ concentration with good precision, lending confidence to the  $\langle [\eta] \rangle_w$  values reported in Table 4. As for cFG, the measured  $\langle M \rangle_w$  is somewhat lower (~7%) than that computed from the sequence, 320,734 (Table 2). While this could be due to the uncertainties in the  $dn/dc$  and extinction coefficients used, which are not known experimentally, it is also possible that the sample has undergone a slight degradation, which we cannot ascertain precisely as done for hHMW-FG and hFrX because of the lack of specific antibodies and limited sample availability. Regarding the  $(\langle R_g^2 \rangle_z)^{1/2}$  values (Table 4), those of cFG and hHMW-FG are very close to each other, and in very good agreement with literature values for unfractionated FG [67, 68]. This confirms the similarity between hHMW-FG and cFG already pointed out from the AUC data analysis (see Results and discussion, Analytical ultracentrifugation). Furthermore, the

lower value for hFrX again hints to a different, more compact shape for this species.

As for  $\langle [\eta] \rangle_w$ , our value for hHMW-FG is ~9% higher than the “best average” literature value [4,66], but values for bovine FG of 27–30 cm<sup>3</sup> g<sup>-1</sup> have been also reported [66]. Since the  $\langle [\eta] \rangle_w$  value drops sharply to ~21 cm<sup>3</sup> g<sup>-1</sup> for our hFrX preparations, it is conceivable that the accepted 25 cm<sup>3</sup> g<sup>-1</sup> for unfractionated FG could result from the contribution of species with degraded  $\alpha C$  regions, although a 60:40 hHMW-FG:hFrX ratio would be required to achieve that value. No literature data are available, to the best of our knowledge, for  $[\eta]$  of cFG and hFrX; our data follow the trend seen with the AUC results, confirming that intact human and chicken FG have pretty much the same overall shape in solution, with minimal influence by the extra  $\alpha C$  repeats.

## Conclusions

In this study, we have presented an in depth analysis of the overall solution conformation of fibrinogen. In particular, we have tried to assess the role of the  $\alpha C$  regions, by examining three well-characterized species differing in the length of this elusive domain. Although the existence of structured and/or interacting stretches cannot be ascertained with our methods, the nearly identical shape parameters for hHMW-FG and cFG, differing by the presence/absence of the 11/12 repeats, suggests that the  $\alpha C$  regions might not be completely “free-swimming” in solution [3,7]. Otherwise, it could have been expected that the lack of a sizeable “connector” would have induced a larger decrease in  $(\langle R_g^2 \rangle_z)^{1/2}$ ,  $R_s$  and  $\langle [\eta] \rangle_w$  between hHMW-FG and cFG. The more dramatic change in these parameters when the bulk of the  $\alpha C$  regions are removed in the hFrX samples, suggests instead that a transition affecting the shape of the main FG body might be involved, influencing also the intermolecular interactions. While the latter effect could be mainly due to the presence/absence of the  $\alpha C$  regions, the shape changes could involve the connectors’ regions. For instance, different degrees of bending at the coiled-coils level were observed in crystals between the various FG species, and even within the same crystals (see [35], and references therein). The presence/absence of the  $\alpha C$  regions could favor alternative conformations, and thus affect FG’s solution behavior. In this respect, the macromolecular solution parameters that we have provided with our study will be of help in discriminating between different models in multi-resolution studies of fibrinogen structure that are currently undergoing in our laboratories.

## Acknowledgments

We are indebted to R.F. Doolittle for his generous gift of chicken fibrinogen, and for providing countless bits of precious information. The expert advice of G. Damonte (University of Genova, Italy) in the mass spectrometry analyses is gratefully acknowledged. Insightful conversations with A. Rowe (University of Nottingham, UK) were also appreciated. This work was partially supported by the Italy–USA project “Farmacogenomics oncology – Oncoproteomics” (Grant 527B/2A/3) to M.R., S.E.H. and G.M. acknowledge

the support of the United Kingdom Biotechnology and Biological Sciences Research Council.

## Appendix A. Supplementary data

Supplementary data associated with this article can be found, in the online version, at doi:10.1016/j.abb.2009.10.008.

## References

- [1] R.F. Doolittle, The molecular biology of fibrin, in: G. Stamatoyannopoulos, P.W. Majerus, R.M. Perlmutter, H. Varmus (Eds.), *The Molecular Basis of Blood Diseases*, third ed., Saunders, Philadelphia, 2000, pp. 719–739.
- [2] B. Blombäck, *Thromb. Res.* 83 (1996) 1–75.
- [3] R.F. Doolittle, *Annu. Rev. Biochem.* 53 (1984) 195–229.
- [4] J.W. Weisel, *Adv. Protein Chem.* 70 (2005) 247–299.
- [5] R.F. Doolittle, D.M. Goldbaum, L.R. Doolittle, *J. Mol. Biol.* 120 (1978) 311–325.
- [6] G. Spraggon, S.J. Everse, R.F. Doolittle, *Nature* 389 (1997) 455–462.
- [7] Z. Yang, J.M. Kollman, L. Pandi, R.F. Doolittle, *Biochemistry* 40 (2001) 12515–12523.
- [8] M.W. Mosesson, J. Hainfeld, J. Wall, R.H. Haschemeyer, *J. Mol. Biol.* 153 (1981) 695–718.
- [9] L.V. Medved', O.V. Gorkun, P.L. Privalov, *FEBS Lett.* 160 (1983) 291–295.
- [10] H.P. Erickson, S. Yakovlev, G. Tsurupa, O.V. Gorkun, L. Medved, J.W. Weisel, Molecular Biology of Fibrinogen and Fibrin, *Annals of the New York Academy of Sciences*, vol. 408, New York Academy of Sciences, New York, 1983, pp. 146–163.
- [11] J.W. Weisel, C.V. Stauffacher, T.E. Bullitt, C. Cohen, *Science* 230 (1985) 1388–1391.
- [12] Y.I. Veklich, O.V. Gorkun, L.V. Medved, W. Nieuwenhuizen, J.W. Weisel, *J. Biol. Chem.* 268 (1993) 13577–13585.
- [13] R.I. Litvinov, S. Yakovlev, G. Tsurupa, O.V. Gorkun, L. Medved, J.W. Weisel, *Biochemistry* 46 (2007) 9133–9142.
- [14] R.F. Doolittle, K.W.K. Watt, B.A. Cottrell, D.D. Strong, M. Riley, *Nature* 280 (1979) 464–468.
- [15] G.R. Crabtree, C.M. Comeau, D.M. Fowlkes, A.J. Fornace Jr., J.D. Malley, J.A. Kant, *J. Mol. Biol.* 185 (1985) 1–19.
- [16] M.W. Rixon, W.-Y. Chan, E.W. Davie, D.W. Chung, *Biochemistry* 22 (1983) 3237–3244.
- [17] J.H. Sobel, C.A. Thibodeau, M.A. Kolks, R.E. Canfield, *Biochemistry* 29 (1990) 8907–8916.
- [18] L. Weissbach, G. Grieninger, *Proc. Natl. Acad. Sci. USA* 87 (1990) 5198–5202.
- [19] M. Murakawa, T. Okamura, T. Kamura, T. Shibuya, M. Harada, Y. Niho, *Thromb. Haemost.* 69 (1993) 351–360.
- [20] M. Murakawa, UniProtKB/Swiss-Prot entry P02672, Nucleotide Sequence [genomic DNA] of bovine fibrinogen alpha chain 174–577, submitted (Sep-1998) to the EMBL/GenBank/DBJ databases.
- [21] A. Henschen, F. Lottspeich, M. Kehl, C. Southan, Covalent structure of fibrinogen, in: M.W. Mosesson, R.F. Doolittle (Eds.), *Molecular Biology of Fibrinogen and Fibrin*, *Annals of the New York Academy of Sciences*, vol. 408, New York Academy of Sciences, New York, 1983, pp. 28–43.
- [22] O. Poirot, E. O'Toole, C. Notredame, *Nucleic Acids Res.* 31 (2003) 3503–3506.
- [23] C. Cole, J.D. Barber, G.J. Barton, *Nucleic Acids Res.* 36 (Web Server issue) (2008) W197–W201.
- [24] D.W. Chung, B.G. Que, M.W. Rixon, M. Mace Jr., E.W. Davie, *Biochemistry* 22 (1983) 3244–3250.
- [25] M.W. Rixon, D.W. Chung, E.W. Davie, *Biochemistry* 24 (1985) 2077–2086.
- [26] V.J. Marder, N.R. Shulman, W.R. Carroll, *J. Biol. Chem.* 244 (1969) 2111–2119.
- [27] T. Takagi, R.F. Doolittle, *Biochemistry* 14 (1975) 940–946.
- [28] M.W. Mosesson, S. Sherry, *Biochemistry* 5 (1966) 2829–2835.
- [29] V.C. Yee, K.P. Pratt, H.C.F. Cote, I. Letrong, D.W. Chung, E.W. Davie, R.E. Stenkamp, D.C. Teller, *Structure* 5 (1997) 125–138.
- [30] J.H. Brown, N. Volkmann, G. Jun, A.H. Henschen-Edman, C. Cohen, *Proc. Natl. Acad. Sci. USA* 97 (2000) 85–90.
- [31] J. Madrazo, J.H. Brown, S. Litvinovich, R. Dominguez, S. Yakovlev, L. Medved, C. Cohen, *Proc. Natl. Acad. Sci. USA* 98 (2001) 11967–11972.
- [32] I. Pechik, J. Madrazo, M.W. Mosesson, I. Hernandez, G.L. Gilliland, L. Medved, *Proc. Natl. Acad. Sci. USA* 101 (2004) 2718–2723.
- [33] M.S. Kostelansky, B. Bolliger-Stucki, L. Betts, O.V. Gorkun, S.T. Lord, *Biochemistry* 43 (2004) 2465–2474.
- [34] R.F. Doolittle, *J. Thromb. Haemost.* 2 (2004) 683–689.
- [35] J.M. Kollman, L. Pandi, M.R. Sawaya, M. Riley, R.F. Doolittle, *Biochemistry* 48 (2009) 3877–3886.
- [36] G. Tsurupa, L. Tsonev, L. Medved, *Biochemistry* 41 (2002) 6449–6459.
- [37] R.A. Burton, G. Tsurupa, L. Medved, N. Tjandra, *Biochemistry* 45 (2006) 2257–2266.
- [38] R.A. Burton, G. Tsurupa, R.R. Hantgan, N. Tjandra, L. Medved, *Biochemistry* 46 (2007) 8550–8560.
- [39] E. Mihalyi, *Biochemistry* 7 (1968) 208–223.
- [40] B. Spotorno, L. Piccinini, G. Tassara, C. Ruggiero, M. Nardini, F. Molina, M. Rocco, *Eur. Biophys. J.* 25 (1997) 373–384 (Erratum 26 (1997) 417).
- [41] U.K. Laemmli, *Nature* 227 (1970) 680–685.
- [42] P.W. Koppert, C.M.G. Huijsmans, W. Nieuwenhuizen, *Blood* 66 (1985) 503–507.
- [43] T.M. Odrjijn, B.J. Rybarczyk, C.W. Francis, S.O. Lawrence, M. Hamaguchi, P.J. Simpson-Haidaris, *Biochim. Biophys. Acta* 1298 (1996) 69–77.
- [44] A. Profumo, M. Turci, G. Damonte, F. Ferri, D. Magatti, B. Cardinali, C. Cuniberti, M. Rocco, *Biochemistry* 42 (2003) 12335–12348.
- [45] I.A. Van Ruijven-Vermeer, W. Nieuwenhuizen, *Biochem. J.* 169 (1978) 653–658.
- [46] B. Holm, D.W.T. Nilsen, P. Kierulf, H. Godal, *Thromb. Res.* 37 (1985) 165–176.
- [47] C.S. Ramarao, D.L. Garbers, *J. Biol. Chem.* 263 (1988) 1524–1529.
- [48] W.F. Stafford, Analytical Ultracentrifugation. Sedimentation Velocity Analysis, *Current Protocols in Protein Science*. 20.7.1–20.7.11, John Wiley & Sons, New York, 2003.
- [49] S.E. Harding, Analysis of polysaccharide size, shape and interactions, in: D.J. Scott, S.E. Harding, A.J. Rowe (Eds.), *Analytical Ultracentrifugation Techniques and Methods*, Royal Society of Chemistry, Cambridge, 2005, pp. 231–252.
- [50] G. Ralston, Introduction to Analytical Ultracentrifugation, Beckman Instruments Inc., Palo Alto, CA, 1993, pp. 27–28.
- [51] N. Gralén, Sedimentation and Diffusion Measurements on Cellulose and Cellulose Derivatives, PhD Dissertation, University of Uppsala, Sweden, 1944.
- [52] A.J. Rowe, *Biopolymers* 16 (1977) 2595–2611.
- [53] W.F. Stafford, P.J. Sherwood, *Biophys. Chem.* 108 (2004) 231–243.
- [54] S. Bernocco, F. Ferri, A. Profumo, C. Cuniberti, M. Rocco, *Biophys. J.* 79 (2000) 561–583.
- [55] G.E. Perlmann, L.G. Longworth, *J. Am. Chem. Soc.* 70 (1948) 2719–2724.
- [56] G.V. Schulz, H.A. Ende, *Z. Phys. Chem.* 36 (1963) 82–96.
- [57] H. Zhu, D.W. Ownby, C.K. Riggs, N.J. Nolasco, J.K. Stoops, A.F. Riggs, *J. Biol. Chem.* 271 (1996) 30007–30021.
- [58] T.L. McMeekin, M. Wilensky, M.L. Groves, *Biochem. Biophys. Res. Commun.* 7 (1962) 151–156.
- [59] V. Ball, J.J. Ramsden, *Biopolymers* 46 (1998) 489–492.
- [60] E. Mihalyi, Kinetics and molecular mechanism of the proteolytic fragmentation of fibrinogen, in: M.W. Mosesson, R.F. Doolittle (Eds.), *Molecular Biology of Fibrinogen and Fibrin*, *Ann. New York Acad. Sci.*, vol. 408, 1983, pp. 60–70.
- [61] S.O. Brennan, *Thromb. Haemost.* 78 (1997) 1055–1058.
- [62] G. Dietler, P. Wiltzius, P. Grolimund, W. Kanzig, A. Haberli, P.W. Straub, Early plasmin digestion of fibrinogen: light scattering data, in: *Fibrinogen – Structure, Functional Aspects, Metabolism*, vol. 2, Walter de Gruyter & Co., Berlin–New York, 1983, pp. 19–23.
- [63] G.R. Palmer, O.G. Fritz, F.R. Hallett, *Biopolymers* 18 (1979) 1647–1658.
- [64] M.W. Mosesson, N. Alkjaersing, B. Sweet, S. Sherry, *Biochemistry* 6 (1967) 3279–3287.
- [65] R.F. Doolittle, *Adv. Prot. Chem.* 27 (1973) 1–109.
- [66] H.A. Scheraga, M. Laskowski Jr., *Adv. Prot. Chem.* 12 (1957) 1–131.
- [67] K. Lederer, R. Hammel, *Makromol. Chem.* 176 (1975) 2619–2639.
- [68] M. Rocco, E. Infusini, M.G. Daga, L. Gogioso, C. Cuniberti, *EMBO J.* 6 (1987) 2343–2349.